SCIENCE CHINA
Information Sciences

• MOOP •

June 2017, Vol. 60 063201:1–063201:8
doi: 10.1007/s11432-017-9077-1

Development of an autonomous flapping-wing aerial vehicle

Wei HE[1], Haifeng HUANG[1], Yunan CHEN[1], Wenzhen XIE[1], Fusen FENG[1], Yemeng KANG[1] & Changyin SUN[2*]

[1]*School of Automation and Electrical Engineering, University of Science and Technology Beijing, Beijing* 100083*, China;*
[2]*School of Automation, Southeast University, Nanjing* 210096*, China*

Received January 25, 2017; accepted April 24, 2017; published online May 19, 2017

Abstract The flapping-wing aerial vehicle (FWAV) has appealed to more and more researchers recently owing to its outstanding performance in various domains and the development of some related technologies. The research on autonomous flight control of the FWAV involves many challenges and is still in nascent stages. In this work, we develop an FWAV with a mass of 14.1 g and build a vision-based experimental platform. A model-based controller is proposed on the basis of theory and simulation results prove its effectiveness. A PID control algorithm based on visual measurement is utilized to achieve the height-keeping control of the FWAV, and a software platform is designed to record the flight status determined using Euler angles and position information.

Keywords flapping-wing aerial vehicle, autonomous robot, control design, vision-based control, unmanned aerial vehicle

Citation He W, Huang H F, Chen Y N, et al. Development of an autonomous flapping-wing aerial vehicle. Sci China Inf Sci, 2017, 60(6): 063201, doi: 10.1007/s11432-017-9077-1

1 Introduction

In the past decades, unmanned aerial vehicles (UAVs) have been widely used in military and civil applications [1]. Traditional UAVs that include fixed-wing aircrafts, unmanned rotorcraft, and unmanned airships find a wide range of applications and play an important role in our modern life. Nevertheless, they are not flexible enough to execute tasks in complicated environments such as narrow spaces. They are also poor at low-altitude flying and have the problem of high power consumption. To apply the UAVs more efficiently and conveniently to practice, various types of FWAVs inspired by insects and birds have been invented. Festo in Germany designed an FWAV named SmartBird inspired by a seagull [2]. SmartBird's body mass is up to 400 g and its wingspan is 2 m. Julian et al. [3] at the University of California, Berkeley designed a micro FWAV named H2bird. The FWAV made of a carbon fiber weighs 13 g and can be loaded with 2.8 g. It uses a glider and flapping wings. The special design of a motor and an elevator at the tail of the FWAV improve its flexibility greatly. Delft University of Technology researchers investigated an FWAV named DelFly [4] in 2005. The first generation

* Corresponding author (email: cysun@seu.edu.cn)

FWAV, DelFly I, weighed 21 g and was built according to a dragonfly model. Compared with the first generation, DelFly II was successfully developed with a reduced mass of 16 g. DelFly II uses lighter electronic devices and a brushless motor instead of the brushed motor, and it can carry a camera while flying. Its forward-flying speed is up to 15 m/s and backward-flying speed is 0.5 m/s. Chung et al. with his group at the University of Illinois at Urbana-Champaign (UIUC) developed a bat robot. This FWAV imitates the bat with its combined joint. This system was subsequently simplified by decreasing the degrees of actuation [5]. Park and his team at KonKuk University carried out a research on bionic FWAVs [6]. They investigated the dynamics analysis, optimization design of bionic structures, and control of the flight altitude. They designed a micro FWAV with a mass of 7.4 g and a wingspan of 1.2 cm that performed perfectly in flight. A Harvard University team named Wood exploited an insect-scale flight robot [7]. To reduce its weight, all structures of this robot, including electronic components, adopt single chip microcomputer technology and the whole robot weighs only 80 mg and is 3 cm in length.

Though many kinds of FWAVs have been developed, the study on autonomous flight control of FWAVs is still in early stages. Traditional flight control techniques such as deterministic learning-enhanced neutral networks in [8] and global neural dynamic surface-tracking control in [9] are effective but do not seem appropriate for FMAVs because of the difference of the models. The main challenges associated with the flight control of the FWAVs can be outlined as follows.

(i) The FWAV is a highly coupled multi-input and multi-output (MIMO) system. Generally speaking, the number of actuators is limited because of the structure, meaning that the system is usually highly underactuated.

(ii) As the wings are flexible, the problem of vibrations caused by high-frequency flapping cannot be ignored [10, 11]. Moreover, an ineluctable small phase lag between two flapping wings exists that will produce undesirable lateral acceleration and a yaw moment.

(iii) The modeling of an FWAV is notoriously difficult as the aerodynamics involved is complex and because the FWAV can be easily influenced by the disturbance from the environment. Without a good model, the design of the control algorithm is challenging.

In this study, we have designed an FWAV with a mass of 14.1 g and a wingspan of 20 cm. With an external vision-based localization system used as an altitude sensor, we have successfully achieved closed-loop height regulation of the FWAV.

In what follows, Section 2 describes the FWAV platform in detail. Section 3 represents the design of the model-based control. Simulation results that prove the validity and rationality of the control law used are also presented. In Section 4, the experiment conducted on the FWAV is explained. Lastly, conclusion is drawn in Section 5.

2 The FMAV platform

The FWAV used in our study is shown in Figure 1. From [12], we know that FWAVs with the X-wing has a lower power requirement compared to FWAVs with a single pair of wings or two wings in tandem. Moreover, this FWAV gives minimal rocking amplitude. The FWAV model in our work is equipped with the X-wing configuration as shown in Figure 2; the FWAV has a mass of 14.1 g and a wingspan of 20 cm. Through the use of a gear box and four connecting rod mechanisms, the FWAV can flap the wings in unison to produce consistent wing lift and thrust.

Given the constraints of mass and size, the components of the FWAV should be chosen carefully. The inner control board of the FWAV is shown in Figure 3. As shown in Figure 4, the control board consists of a 32-bit ARM-based Cortex-M3 microprocessor STM32L151, which has ultralow power consumption, a Bluetooth to send and receive detection information, a motion sensor that includes a 3-axis accelerometer, a 3-axis gyroscope, and a 3-axis magnetic induction sensor, a barometer, a status indicator lamp, a power module, and a motor drive. During the flight, the control board receives the relative height signal measured by the vision measurement system and generates control signals for the motor to drive the FWAV. The radio transceiver is only used to communicate detection signals and flight status information.

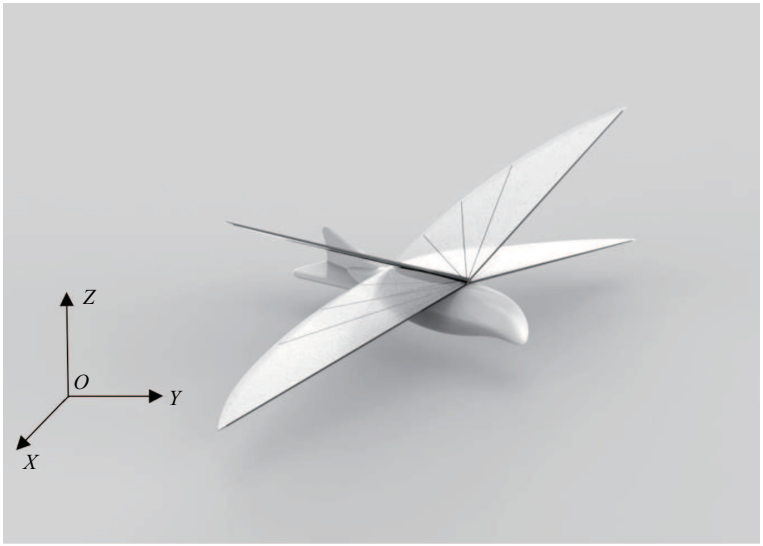

Figure 1 The designed 3D model of the FWAV.

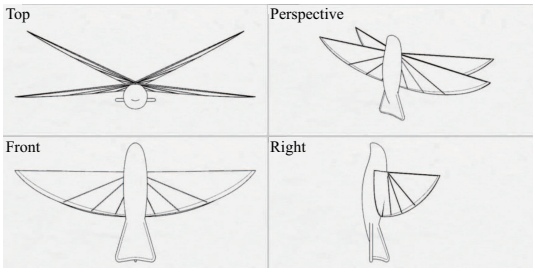

Figure 2 The structure of the X-wing.

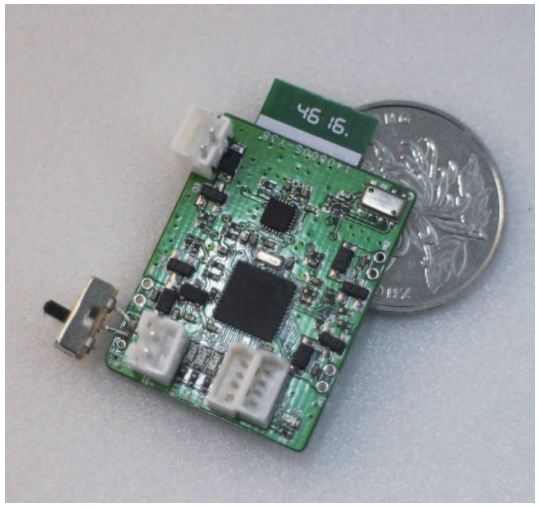

Figure 3 (Color online) The designed control circuit board.

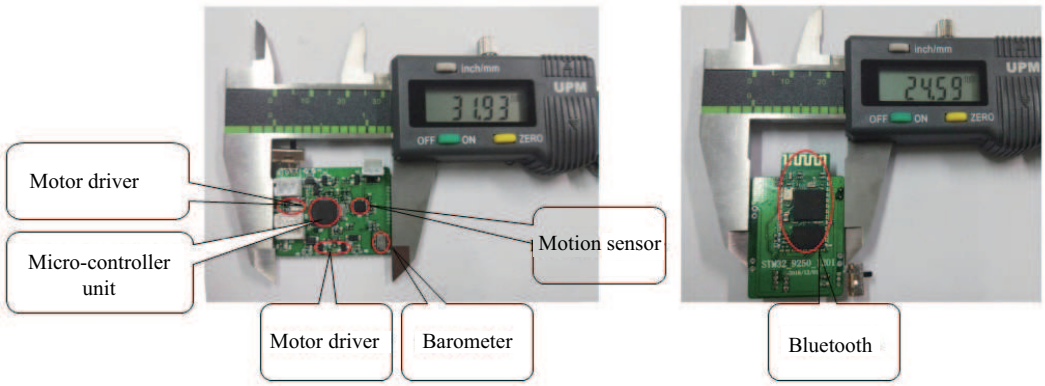

Figure 4 (Color online) Functional modules of the control circuit board.

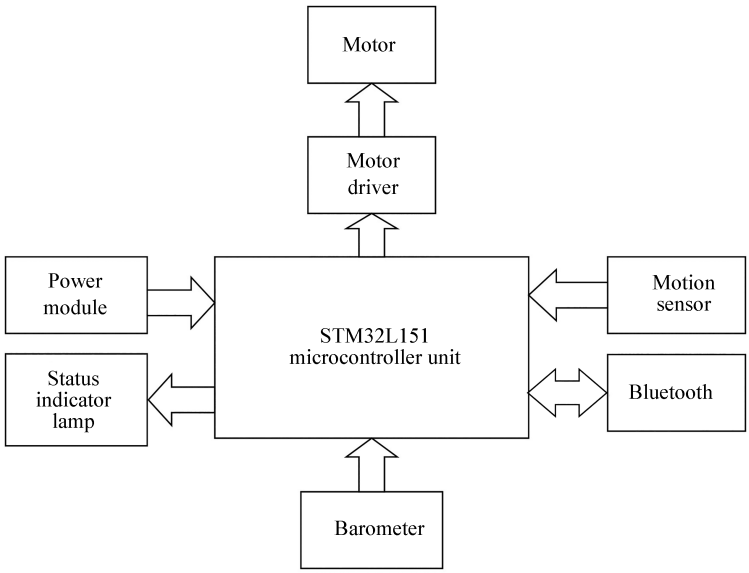

Figure 5 Communication among various modules of the control circuit board.

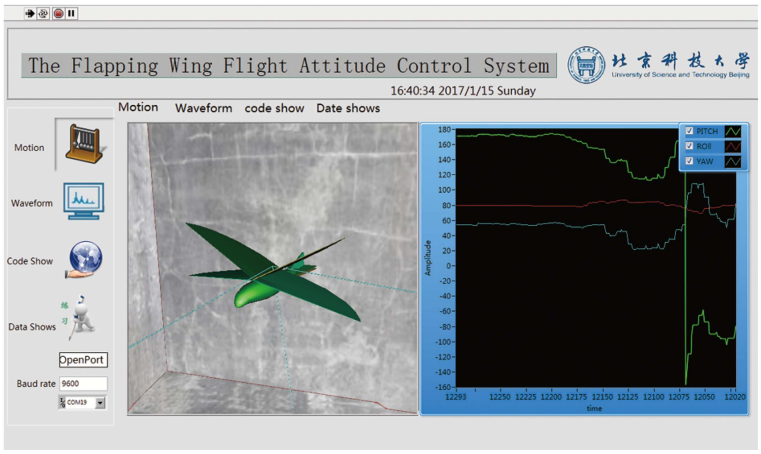

Figure 6 (Color online) The altitude display software platform.

Figure 5 shows the communication between the components of the control board.

The flight control board weighs approximately 3.2 g and is 31.9 mm × 24.4 mm in size. It contains a 32-bit STM32l151 microprocessor running at 36 MHz. The microprocessor is used for a range of robotic applications that require multiple peripherals. We use two I^2C channels, two UART channels, and four PWM channels. An internal SRAM of 16 KB capacity is mainly used for caching the data temporarily received or to be sent via Bluetooth communications. Real-time data such as the sensor output, quaternion and Euler angles after operation, motor output state estimation, and control input are sent to the computer through Bluetooth, and then visualized through 3D modeling and visualization plug-ins as shown in Figure 6. Real-time monitoring is realized and the flight status is stored for post-data analysis and algorithm optimization.

A complete communication network is implemented by using two HC06 Bluetooth modules. HC06 is a high-performance master-slave Bluetooth serial port module that can be used for communicating with an intelligent terminal such as a computer, mobile phone, or a PDA. The module supports a very wide baud rate that ranges from 4800 bit/s to 1382400 bit/s. It is compatible with a 5 V or 3.3 V microcontroller system, and has a built-in 2.4 GHz antenna.

3 Control design

The dynamics of the FWAV with regard to altitude and position control is described as [13]

$$M(q)\ddot{q} + C(q,\dot{q})q + G = R(q)u_c(t) + d(t). \tag{1}$$

Considering only the position, the equation can be written as

$$M_t(q_t)\ddot{q}_t + G_t + d_t(t) = R^{\mathrm{IB}}(q_r)u_t, \tag{2}$$

where $q_t = [x, y, z]^{\mathrm{T}}$ indicates the position variables in the inertial coordinate system,

$$M_t = \begin{bmatrix} m & 0 & 0 \\ 0 & m & 0 \\ 0 & 0 & m \end{bmatrix}$$

is the mass matrix, $G_t = [0, 0, -mg]^{\mathrm{T}}$ is the gravity vector, $d_t(t)$ is the disturbance, and u_t is the position controller input. $R^{\mathrm{IB}}(q_r)$ is the rotation matrix from the inertial coordinate system to the body coordinate system and satisfies $R^{\mathrm{IB}}(q_r(t)) = (R^{\mathrm{BI}}(q_r(t)))^{-1}$. Its inverse matrix is defined as

$$R^{\mathrm{BI}}(q_r(t)) = \begin{bmatrix} 1 & 0 & 0 \\ 0 & \cos(\theta_1) & \sin(\theta_1) \\ 0 & -\sin(\theta_1) & \cos(\theta_1) \end{bmatrix} \times \begin{bmatrix} \cos(\theta_2) & 0 & -\sin(\theta_2) \\ 0 & 1 & 0 \\ \sin(\theta_2) & 0 & \cos(\theta_2) \end{bmatrix} \times \begin{bmatrix} \cos(\theta_3) & \sin(\theta_3) & 0 \\ -\sin(\theta_3) & \cos(\theta_3) & 0 \\ 0 & 0 & 1 \end{bmatrix}. \tag{3}$$

Let $x_{t1} = q_t = [x, y, z]^{\mathrm{T}}$, $x_{t2} = \dot{q}_t = [\dot{x}, \dot{y}, \dot{z}]^{\mathrm{T}}$. $q_r = [\theta_1, \theta_2, \theta_3]^{\mathrm{T}}$ are the Euler angles in the body coordinate system that can be known from altitude calculation. Then we can describe the robot dynamics as follows:

$$\dot{x}_{t1} = x_{t2}, \tag{4}$$

$$\dot{x}_{t2} = M_t^{-1}\left[R^{\mathrm{IB}}(q_r)u_t - d_t(t) - G_t\right]. \tag{5}$$

The control objective is to design control torques such that the system variable x_1 tracks the given desired trajectories $x_{t1\mathrm{d}}(t) = [x_{\mathrm{d}}(t), y_{\mathrm{d}}(t), z_{\mathrm{d}}(t)]^{\mathrm{T}}$, while ensuring that all closed-loop signals are bounded.

Therefore, we consider the case where full state information x_{t1} and x_{t2} are available and define

$$z_{t1} = x_{t1} - x_{t1\mathrm{d}}, \tag{6}$$

$$z_{t2} = x_{t2} - \alpha_{t1}, \tag{7}$$

where $\alpha_{t1} = \dot{x}_{t1\mathrm{d}} - k_1 z_1$ is a virtue controller.

Now, we can write

$$\dot{z}_{t1} = \dot{x}_{t1} - \dot{x}_{t1\mathrm{d}} = x_{t2} - \dot{x}_{t1\mathrm{d}} = z_{t2} + \alpha_{t1} - \dot{x}_{t1\mathrm{d}}, \tag{8}$$

$$\dot{z}_{t2} = \dot{x}_{t2} - \dot{\alpha}_{t1} = M_t^{-1}\left[R^{\mathrm{IB}}(q_r)u_t - d_t(t) - G_t\right] - \dot{\alpha}_{t1}. \tag{9}$$

To demonstrate the stability of the designed controller, we consider a Lyapunov function of the following form:

$$V = \frac{1}{2}z_{t1}^{\mathrm{T}}z_{t1} + \frac{1}{2}z_{t2}^{\mathrm{T}}M_t z_{t2}. \tag{10}$$

Differentiating V with respect to time, we have

$$\dot{V} = z_{t1}^{\mathrm{T}}\dot{z}_{t1} + z_{t2}^{\mathrm{T}}M_t z_{t2} = z_{t1}^{\mathrm{T}}z_{t2} + \alpha_{t1} - \dot{x}_{t1\mathrm{d}} + z_{t2}^{\mathrm{T}}\left[R^{\mathrm{IB}}(q_r)u_t - d_t(t) - G_t - M_t\dot{\alpha}_{t1}\right]. \tag{11}$$

We assume that the disturbance $d_t(t)$ is bounded, i.e., $\bar{d}(t) \in \mathbb{R}^+$ is a constant and $|d(t)| \leqslant \bar{d}(t), \forall t \in [0, \infty)$. As M_t and G_t are known, the model-based controller is proposed as

$$u_t = \left(R^{\mathrm{IB}}(q_r)\right)^{-1}\left[-z_{t1} - K_2 z_{t2} - \mathrm{sgn}\left(z_{t2}^{\mathrm{T}}\right)\bar{d}_t(t) + G_t + M_t\dot{\alpha}_{t1}\right], \tag{12}$$

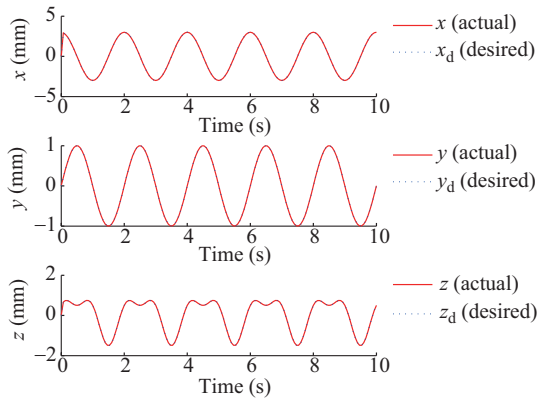

Figure 7 (Color online) Tracking performance.

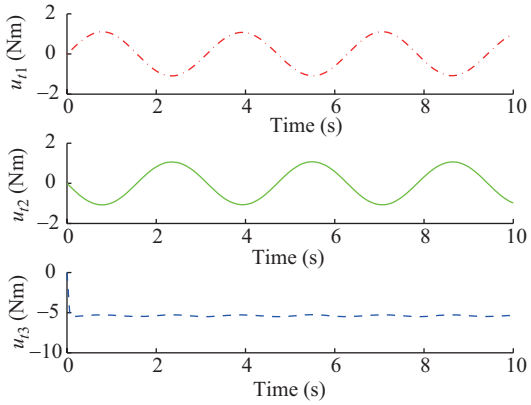

Figure 8 (Color online) Control inputs.

where sgn(·) denotes the signs of the homologous elements of the vector (·) and the gain matrix $K_2 = K_2^{\mathrm{T}} > 0$. Then, we have

$$\dot{V} \leqslant -z_{t1}^{\mathrm{T}} K_1 z_{t1} - z_{t2}^{\mathrm{T}} K_2 z_{t2} \leqslant 0. \tag{13}$$

Only when $z_{t1} = z_{t2} = 0$ can $V(t)$ be zero. According to Barbalat's lemma [14, 15], we know that the signals z_{t1} and z_{t1} are uniformly asymptotically stable. To verify the effectiveness of the proposed control, we carry out some extensive simulations. We assume that the altitude feedback from the motion sensor is $\theta = [\theta_1, \theta_2, \theta_3]^{\mathrm{T}} = [0.2\sin(2t), 0.2\sin(2t), 0.2\sin(2t)]^{\mathrm{T}}$. The desired trajectories of x_{t1} are set as follows:

$$\begin{cases} x_{\mathrm{d}} = 3\cos(\pi t), \\ y_{\mathrm{d}} = \sin(\pi t), \\ z_{\mathrm{d}} = \sin(\pi t) + 0.5\cos(2\pi t). \end{cases} \tag{14}$$

We choose $K_1 = \mathrm{diag}[100, 100, 100]$ and $K_2 = \mathrm{diag}[80, 80, 80]$. The simulation results are shown in Figures 7 and 8, from which we can see that the outputs can track the desired trajectories successfully and the inputs are appropriate.

4 Experiment

To verify the effectiveness of the FWAV platform developed, we conducted an indoor flight test on the FWAV. The experimental architecture and the experimental scene graph are shown in Figures 9 and 10, respectively. Using an external vision-based localization system as an altitude sensor, we designed an experiment to achieve closed-loop height-keeping flight of the FWAV. To avoid any damage to the FWAV and make sure that it will not fly out of the measurable range, we used a rope and a hook to hang the aircraft. The Vicon composite motion capture system was used as the vision-based localization system. We attached three reflective markers on the FWAV's body that could be identified by 12 cameras, to return the location information of the FWAV to the computer. The real-time position of the FWAV is represented by the coordinate values (x, y, z). Through Bluetooth, we sent the actual height z and the desired height z_{d} from the computer to the control board, and the coordinate values were recorded in the computer. We adopted the PID control method to realize the height-keeping flight of the FWAV. The error is the difference between the desired height and the actual height values of the FWAV, i.e., $e(t) = z_{\mathrm{d}} - z$. The expression of the used PID algorithm is $u(t) = K_{\mathrm{p}} e(t) + K_{\mathrm{I}} \int_0^t e(t)\mathrm{d}t + K_{\mathrm{d}} \frac{\mathrm{d}e(t)}{\mathrm{d}t}$.

The experimental results are illustrated in Figures 11 and 12 in which the dash-dot line and the dashed line represent the x and y positions respectively. It can be observed that they change periodically as the FWAV is hovering in the space. The solid line indicates the position z. The black dotted line indicates the setting altitude $z_{\mathrm{d}} = 0.75$ m. Within 20 m, the actual altitude coincides with the setting values well

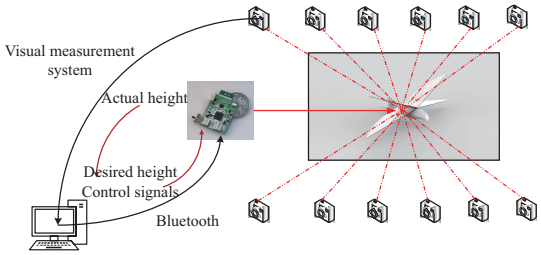

Figure 9 (Color online) Architecture of the vision-based height-keeping control system.

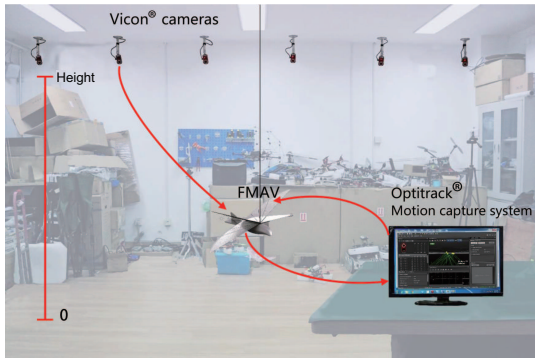

Figure 10 (Color online) Vicon motion capture system with multiple cameras.

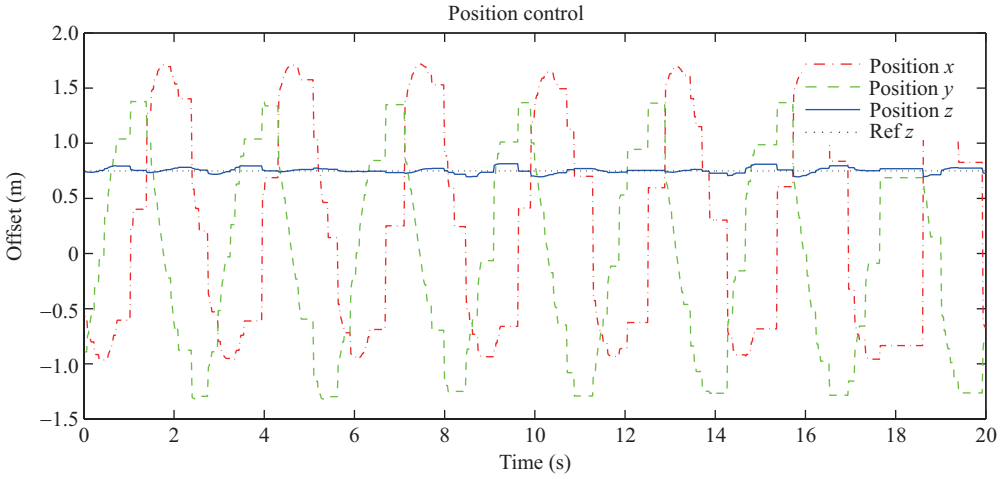

Figure 11 (Color online) Experimental results of the height-keeping flight: $z_{\rm d} = 0.75$ m.

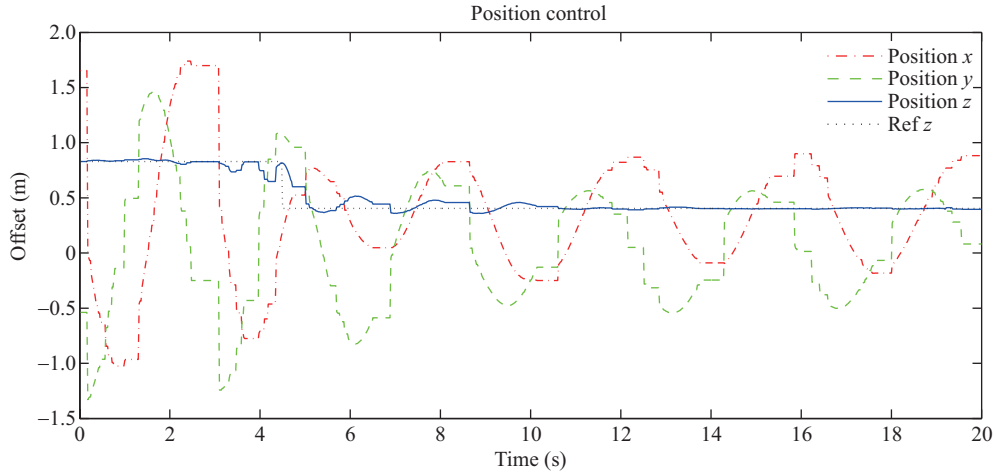

Figure 12 (Color online) Experimental results of the height-keeping flight: $z_{\rm d} = 0.83$ m (0–4.5 s); $z_{\rm d} = 0.4$ m (4.5–20 s).

within the acceptable range. Furthermore, as seen from Figure 12, there is a step signal of setting height $z_{\rm d}$ that changes from 0.83 m to 0.4 m at $t = 4.5$ s. The actual height z reaches the set value within 0.6 m, and it becomes smooth and steady at $t = 10.5$ s.

Figures 11 and 12 illustrate that the FWAV can essentially track the desired height with small errors. The errors are influenced by many factors. We adjusted the frequency of wing flapping by controlling

the motor speed to further control the height, but there is not exactly a linear relationship between the flapping frequency and the height in fact. Until now, the aerodynamic model of the FWAV is not clear enough. The flapping frequency, altitude angles, vibration of the wings, and even the rope used to hang the bird influence the change in the height of the FWAV. In addition, time delays exist during the communication between the PC and the control board as well as the visual measurement system. All of these may have an influence on our experimental results.

5 Conclusion

In this work, we developed an FWAV platform and presented a model-based control law theoretically. Experiments on the height-keeping control of the FWAV through a PID control method showed a good performance, but till now, we can just control the height through a traditional PID control algorithm that is very limited for complex nonlinear systems and complex signal tracking. Our future work will focus on adopting more advanced control algorithms such as those based on adaptive neural network control and trying to control not only the position but also the altitude of the FWAV. Vibration control for the flexible wings is also one of the problems that we are considering to address in the future.

Acknowledgements This work was supported by National Natural Science Foundation of China (Grant Nos. 61522302, 61520106009, 61533008), Beijing Natural Science Foundation (Grant No. 4172041), and Fundamental Research Funds for the China Central Universities of USTB (Grant No. FRF-TP-15-005C1).

Conflict of interest The authors declare that they have no conflict of interest.

Supporting information The supporting information is available online at info.scichina.com and link.springer.com. The supporting materials are published as submitted, without typesetting or editing. The responsibility for scientific accuracy and content remains entirely with the authors.

References

1 Duan H B, Li H, Luo Q N, et al. A binocular vision-based UAVs autonomous aerial refueling platform. Sci China Inf Sci, 2016, 59: 053201
2 Mackenzie D. A flapping of wings. Science, 2012, 335: 1430–1433
3 Julian R C, Rose C J, Hu H, et al. Cooperative control and modeling for narrow passage traversal with an ornithopter MAV and lightweight ground station. In: Proceedings of the 2013 International Conference on Autonomous Agents and Multi-Agent Systems (AAMAS), Minnesota, 2013. 103–110
4 de Croon G C H E, Perçin M, Remes B D W, et al. The DelFly. Berlin: Springer Netherlands, 2016
5 Ramezani A, Chung S J, Hutchinson S. A biomimetic robotic platform to study flight specializations of bats. Sci Rob, 2017, 2: eaal2505
6 Phan H V, Truong Q T, Park H C. Implementation of initial passive stability in insect-mimicking flapping-wing micro air vehicle. Int J Intell Unman Syst, 2015, 3: 18–38
7 Ma K Y, Chirarattananon P, Fuller S B, et al. Controlled flight of a biologically inspired, insect-scale robot. Science, 2013, 340: 603–607
8 Jiang Y, Yang C, Dai S, et al. Deterministic learning enhanced neutral network control of unmanned helicopter. Int J Advanced Robot Syst, 2016, 13: 1–12
9 Xu B, Yang C, Pan Y. Global neural dynamic surface tracking control of strict-feedback systems with application to hypersonic flight vehicle. IEEE Trans Neural Netw Learn Syst, 2015, 26: 2563–2575
10 He W, Zhang S. Control design for nonlinear flexible wings of a robotic aircraft. IEEE Trans Control Syst Tech, 2017, 25: 351–357
11 He W, Lv T, Chen Y, et al. Modeling and vibration control of flexible wings with output constraint. In: Proceedings of the 12th IEEE World Congress on the Intelligent Control and Automation (WCICA), Guilin, 2016. 1141–1146
12 Tay W B, van Oudheusden B W, Bijl H. Numerical simulation of X-wing type biplane flapping wings in 3D using the immersed boundary method. Bioinspir Biomi, 2014, 9: 036001
13 Banazadeh A, Taymourtash N. Adaptive altitude and position control of an insect-like flapping wing air vehicle. Nonlinear Dyn, 2016, 85: 47–66
14 Krstic M, Kanellakopoulos I, Kokotovic P V. Nonlinear and Adaptive Control Design. New York: Wiley, 1995
15 Slotine J J E, Li W. Applied Nonlinear Control. Englewood Cliffs: Prentice-Hall, 1991